Giant Frictional Drag in Double Bilayer Graphene Heterostructures

Kayoung Lee, Jiamin Xue, David C. Dillen, Kenji Watanabe, Takashi Taniguchi, and Emanuel Tutuc

Giant Frictional Drag in Double Bilayer Graphene Heterostructures

Kayoung Lee,[1] Jiamin Xue,[1] David C. Dillen,[1] Kenji Watanabe,[2] Takashi Taniguchi,[2] and Emanuel Tutuc[1]

[1]*Microelectronics Research Center, The University of Texas at Austin, Austin, TX 78758, USA*
[2]*National Institute of Materials Science, 1-1 Namiki Tsukuba, Ibaraki 305-0044, Japan*
(Dated: May 5, 2016)

We study the frictional drag between carriers in two bilayer graphene flakes separated by a $2-5$ nm thick hexagonal boron nitride dielectric. At temperatures (T) lower than ~ 10 K, we observe a large anomalous negative drag emerging predominantly near the drag layer charge neutrality. The anomalous drag resistivity increases dramatically with reducing T, and becomes comparable to the layer resistivity at the lowest $T = 1.5$ K. At low T the drag resistivity exhibits a breakdown of layer reciprocity. A comparison of the drag resistivity and the drag layer Peltier coefficient suggests a thermoelectric origin of this anomalous drag.

Interaction between isolated electron systems in close proximity can produce a wealth of novel phenomena. A particularly striking example is frictional drag where charge current (I_{Drive}) flowing in one (drive) layer induces a voltage drop in the opposite (drag) layer, $V_{\mathrm{Drag}} = R_{\mathrm{D}} I_{\mathrm{Drive}}$. At the heart of the transresistance R_{D} are inter-layer couplings without particle exchange which can be mediated by e.g., momentum exchange [1], energy transfer [2], or phonons [3]. While being a sensitive probe of inter-layer interactions, the R_{D} values are generally much smaller than the layer resistance. An exception occurs when the carriers in the two layers form a correlated state, yielding R_{D} that can reach values comparable to the layer resistance. Indeed, this has been experimentally reported in GaAs electron [4], or hole [5] double layer systems, in magnetic fields such that each layer has one half-filled Landau level [6].

Extensive experimental effort has been devoted to probe drag in electron-hole double layers, using GaAs electron-hole double layers [7, 8], graphene double layers [9, 10], and most recently graphene-GaAs double layers [11], motivated in part by the search for equilibrium indirect exciton condensates. A common thread in these experiments is an anomalous R_D that increases with reducing T, along with a breakdown of layer reciprocity when interchanging the drive and drag layers [7, 8, 11]. In this regard, double bilayer graphene separated by a thin hexagonal boron nitride (hBN) is a particularly compelling system. The near parabolic energy-momentum dispersion in bilayer graphene allows the Coulomb to kinetic energy ratio to be tuned via density, unlike monolayer graphene where this ratio is fixed [12]. Moreover, the availability of ultra-thin dielectrics allows double layers to be realized with interlayer spacing (d) down to a few nm, granting access to the strong coupling regime $d \ll l$, where l is the inter-particle distance. This effectively nests the two isolated electronic systems in the same plane. Here, we investigate the frictional drag in double bilayer graphene heterostructures, consisting of two bilayer graphene separated by a $2-5$ nm thick interlayer hBN dielectric, which allows us to explore the drag in a wide range of layer densities and for all combinations of carrier polarity. Strikingly, we find a giant and negative drag resistivity at charge neutrality, comparable to the layer resistivity at the lowest T.

The samples [Fig. 1(a)] are fabricated using a layer-by-layer transfer process similar to samples discussed in [13]. The layer densities are tuned using a combination of back-gate (V_{BG}), and interlayer bias applied on the top bilayer (V_{TL}) [14]. The top (ρ_{T}) and bottom (ρ_{B}) bilayer resistivities, as well as the frictional drag are probed using small signal, low frequency lock-in techniques. We investigated four samples, labeled A-E, with different interlayer spacing and layer mobilities. The interlayer resistance values are in the range 1.6 - 20 GΩ. The drag resistance measurement errors associated with finite interlayer resistance are of the order 1%. The key features of the drag data discussed below are similar in all samples.

Figures 1(b) and 1(c) show ρ_{B} and ρ_{T} measured in Sample A at $T = 1.5$ K. The bottom bilayer responds to V_{BG} and V_{TL} similar to a dual-gated bilayer graphene, in which the density and transverse electric field (E) are controlled independently [15]. The locus of high resistance points in Figs. 1(b,c) marks the charge neutrality lines for both bilayers. Figure 1(c) also shows the carrier type in each of the four quadrants defined by the two charge neutrality lines. To examine variations in the drag resistance when interchanging the drag and drive layers, we probe both the bottom ($\rho_{\mathrm{D,B}}$) and top ($\rho_{\mathrm{D,T}}$) drag resistivities, with the top or bottom bilayers serving as the drive layers, respectively. Figures 1(d) and 1(e) show $\rho_{\mathrm{D,B}}$ and $\rho_{\mathrm{D,T}}$, respectively, measured as a function of V_{BG} and V_{TL} in Sample A, at $T = 1.5$ K. A comparison of Fig. 1(b,c) data on one hand, and Fig. 1(d,e) data on the other, shows a large, negative drag resistivity emerging predominantly near or at the drag layer charge neutrality.

To better visualize Fig. 1(d,e) data, in Fig. 2 we plot $\rho_{\mathrm{D,B}}$ [panel (a)] and $\rho_{\mathrm{D,T}}$ [panel (b)] as a function of top (n_{T}) and bottom (n_{B}) bilayer densities, converted from V_{BG} and V_{TL}. The n_{T} and n_{B} values are related to the applied V_{BG} and V_{TL} biases, referenced with respect to $n_{\mathrm{B}} = n_{\mathrm{T}} = 0$, via: $eV_{\mathrm{BG}} = e^2(n_{\mathrm{B}} + n_{\mathrm{T}})/C_{\mathrm{BG}} + \mu_{\mathrm{B}}$ and
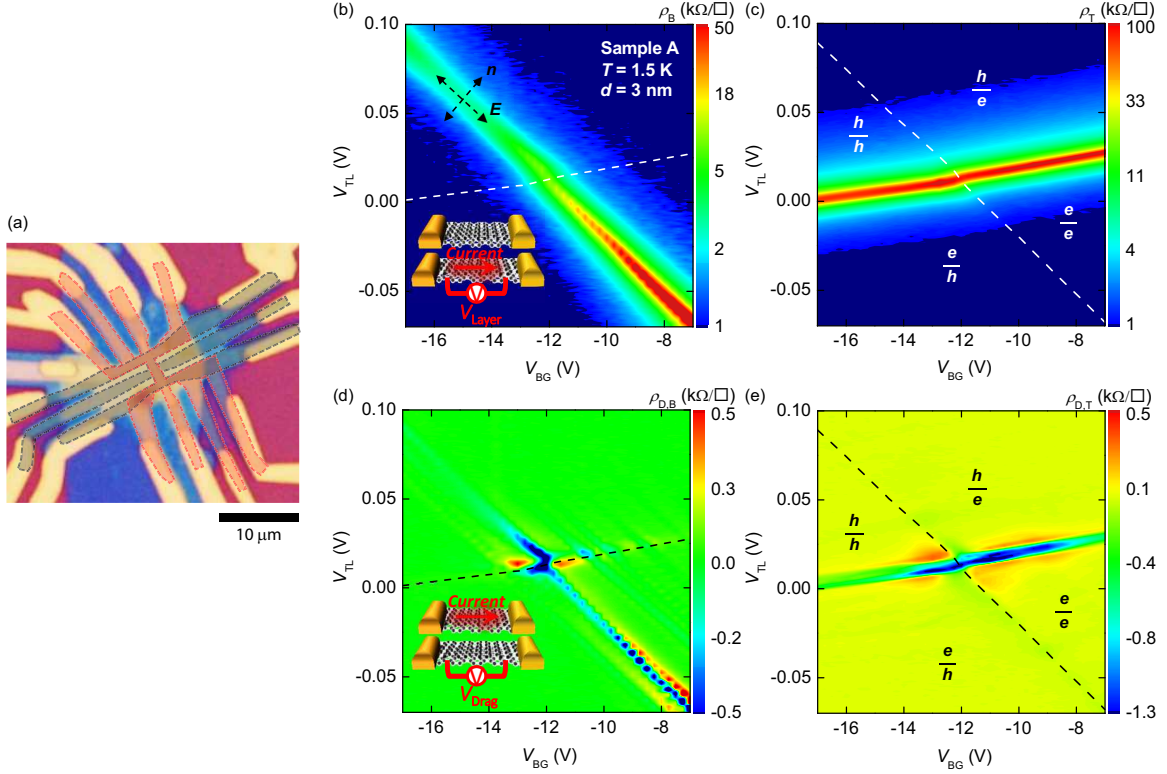
FIG. 1: (a) Optical micrograph of a double bilayer graphene heterostructure. The red (gray) dashed contour lines mark the top (bottom) bilayer. (b) ρ_B, and (c) ρ_T measured in Sample A as a function of V_{BG} and V_{TL} at $T = 1.5$ K. Panel (b) inset shows the sample and measurement schematic. The white dashed lines in panels (b) and (c) mark the charge neutrality lines of the top and bottom bilayers, respectively. Panel (c) shows the carrier type in the two bilayers in the four quadrants defined by the two charge neutrality lines. (d) $\rho_{D,B}$ and (e) $\rho_{D,T}$ measured as a function of of V_{BG} and V_{TL} at $T = 1.5$ K.
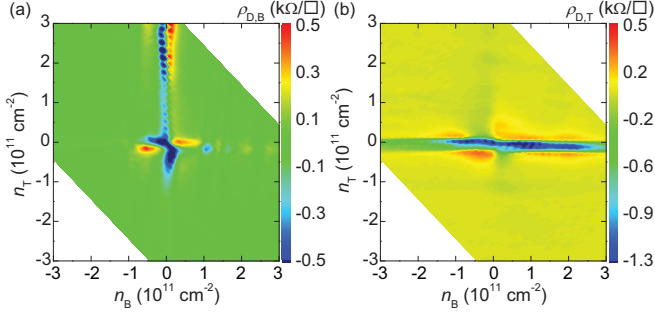

FIG. 2: (a) $\rho_{D,B}$ and (b) $\rho_{D,T}$ as a function of n_B and n_T, measured at $T = 1.5$ K. The data show a large drag resistivity emerging along the drag layer charge neutrality, relatively insensitive to the drive layer density.

$eV_{TL} = -e^2 n_T/C_{int} + \mu_B - \mu_T$, where C_{BG} and C_{int} are the back-gate and interlayer capacitances, μ_T and μ_B are the top and bottom bilayer chemical potentials, respectively, e is the electron charge. To convert V_{BG} and V_{TL} to layer densities we use the density-dependent chemical

potential determined experimentally [13]. The C_{BG} and C_{int} values are determined using magnetotransport measurements of individual bilayers [16]. Figure 2 reveals a number of interesting features. First, $\rho_{D,B}$ is large in the proximity of $n_B = 0$ line in Fig. 2(a), while $\rho_{D,T}$ is large near $n_T = 0$ line in Fig. 2(b). Near the double neutrality point (DNP), $n_B = n_T = 0$ $\rho_{D,B}$ and $\rho_{D,T}$ reach values close to 1 kΩ. Second, the reciprocity with respect to interchanging the drag and drive layers breaks down, i.e. $\rho_{D,B}(n_B, n_T) \neq \rho_{D,T}(n_B, n_T)$ in Fig. 2.

In light of the anomalous drag observed in Figs. 1 and 2, in the following we examine the drag layer resistivity in more detail, concentrating on the drag layer density, and transverse electric field (E) dependencies. The latter is relevant for bilayer graphene as the energy-momentum dispersion changes with E, concomitant with gap opening at charge neutrality [17]. Figure 3(a) shows Sample A ρ_B, $\rho_{D,B}$, and the corresponding normalized drag $\rho_{D,B}/\rho_B$ as a function of $n_B = -n_T$, namely at equal density in the two bilayers, with opposite polarity carriers. $\rho_{D,B}$ shows a very strong, negative peak at DNP, which
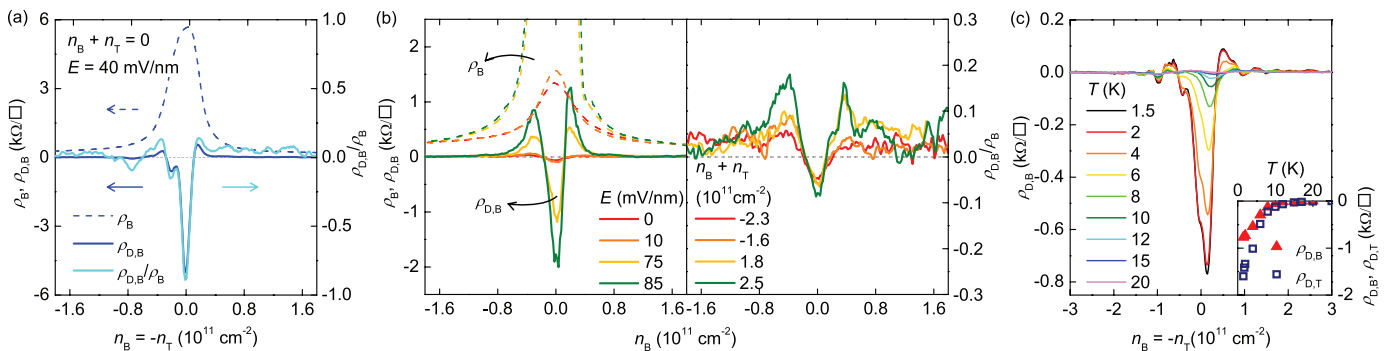
FIG. 3: (a) ρ_B, $\rho_{D,B}$ (left axis), and $\rho_{D,B}/\rho_B$ (right axis) as a function of $n_B = -n_T$, measured at $T = 1.5$ K in Sample A. The $\rho_{D,B}$ and ρ_B values are comparable at DNP. The E-field across the bottom bilayer (drag layer) is 40 mV/nm at DNP. (b) Left panel: ρ_B (dashed lines), and $\rho_{D,B}$ (solid lines) vs. n_B in Sample A at different E values in the bottom bilayer at $T = 1.5$ K. Right panel: $\rho_{D,B}/\rho_B$ vs. n_B corresponding to the left panel data. The data were acquired at constant $n_B + n_T$ total density values. (c) $\rho_{D,B}$ as a function of $n_B = -n_T$, in the proximity of DNP at different T, measured in Sample A in a separate cooldown. The inset shows $\rho_{D,B}$ and $\rho_{D,T}$ vs. T at the DNP.

surprisingly becomes comparable to ρ_B at $T = 1.5$ K. As $n_B = -n_T$ increases $\rho_{D,B}$ changes sign, becomes positive at a finite $|n_B|$, and then vanishes as $|n_B|$ increases further.

Figure 3(b) shows ρ_B, $\rho_{D,B}$ (left panel), and $\rho_{D,B}/\rho_B$ (right panel) vs. n_B in the proximity of $n_B = 0$ and $n_T \neq 0$. The negative $\rho_{D,B}$ at $n_B = 0$ is notable, similar to the large, negative $\rho_{D,B}$ peak at DNP in Fig. 3(a). However, the magnitude of $\rho_{D,B}/\rho_B$ at $n_B = 0$ and $n_T \neq 0$ is smaller than that at DNP. As $|n_B|$ increases, $\rho_{D,B}$ changes polarity, and becomes positive, consistent with the observed trend at DNP, albeit with a lower magnitude. An examination of the electrostatics in double layers shows that at $n_B = 0$, the E value across the bottom bilayer changes as n_T changes as indicated in Fig. 3(b) legend (Supplementary Material). We observe that $\rho_{D,B}$ at $n_B = 0$ grows as ρ_B increases with increasing E-field, leading to a relatively constant $\rho_{D,B}/\rho_B$ ratio.

Figure 3(c) shows $\rho_{D,B}$ as a function of $n_B = -n_T$ at different T in Sample A, showing a large, negative drag at DNP. We note that Fig. 3(a,b) and Fig. 3(c) were collected in separate cooldowns. Similar to Fig. 3(a) data, $\rho_{D,B}$ becomes positive as $|n_B|$ increases, and subsequently decreases towards zero with increasing density. The inset of Fig. 3(c) summarizes the T-dependence of the negative peak of both $\rho_{D,B}$ and $\rho_{D,T}$ at DNP, showing a decrease of the drag resistivity with increasing T. At the lowest T, mesoscopic fluctuations [14] are also noticeable in the proximity of DNP in Fig. 3(c), superimposed onto the large negative drag.

The experimental observations in Figs. 1-3 have several anomalous features at variance with existing Coulomb drag theories. It is tempting to interpret the giant drag that develops at DNP at low T *prima facie* as a signature of a correlated state of the two layers. However, the fact that the drag voltage is negative, namely opposite to the electric field in the drive layer, coupled with

the layer reciprocity breakdown casts doubt on this interpretation. Moreover, the increasing ρ_D observed with decreasing T [Fig. 3(c)] is opposite to the expected dependence for momentum transfer mediated drag [1] . The increasing drag at the lowest T, coupled with the apparent breakdown of reciprocity bears similarity with data reported in electron-hole double layers in GaAs-AlGaAs [7] or GaAs-graphene heterostructures [11]. We note that the interlayer separations in [7, 11] were larger than 10 nm, and the magnitude of the measured drag resistivity was two orders of magnitude smaller than the values probed in the double bilayer graphene heterostructures investigated here. Indeed, the $\rho_{D,B} \approx \rho_B$ is a dramatic signature of the strong coupling regime in double layers.

To gain insight into the origin of the anomalous drag we first note that the $\rho_{D,B}$ and ρ_B peaks in Fig. 3(a) have similar widths. The giant peak at the DNP is reminiscent of energy drag near charge neutrality in double monolayer graphene heterostructures [2, 10], where Coulomb mediated vertical energy transfer coupled with correlated density inhomogeneity in the two layers yields a drag resistivity of thermoelectric origin, with the polarity determined by interlayer correlations $\langle \delta\mu_B \delta\mu_T \rangle$. To assess the role of thermoelectricity in our measurements we use the Mott relation for the Peltier coefficient [18, 19]:

$$Q = \frac{\pi^2 k_B^2 T^2}{3e} \frac{\partial\sigma/\partial\mu}{\sigma} \tag{1}$$

where k_B is the Boltzmann constant, and σ the layer conductivity. Using Eq. (1) along with $\sigma = 1/\rho_B$ measured in the bottom bilayer graphene, the experimental μ vs. n_B data (Fig. S1) [13], and n_B vs. V_{BG} and V_{TL} (Fig. S2), we obtain Q_B vs. μ_B.

In Fig. 4(a) (main panel) we compare the drag layer chemical potential (μ_{Drag}) dependence of ρ_D and drag layer $-\partial Q/\partial\mu$, in Samples A and B at $T = 1.5$ K. The bottom (top) layer serve as drag layer in sample A (B).

The data were measured while sweeping the layer densities such that $n_B = -n_T$. A main difference between the two samples is that the drag layer mobility is 260,000 cm^2/V·s in sample A, as opposed to 19,000 cm^2/V·s in sample B. Remarkably, both ρ_D and $-\partial Q/\partial \mu$ show a peak at charge neutrality, change polarity as $|\mu_{Drag}|$ increases, and vanish at even larger $|\mu_{Drag}|$ values. Interestingly, the peak structure of energy drag in Ref. [2] arises from $\partial Q/\partial \mu$.

The striking similarity between the μ_{Drag}-dependence of ρ_D and $-\partial Q/\partial \mu$ strongly suggests a thermoelectric origin for the large frictional drag observed at low T in our double bilayer graphene. To further test this hypothesis, in Fig. 4(b) we compare the μ_{Drag} value at which ρ_D changes polarity ($|\mu_{Drag=0}|$), and the μ value at which the drag layer $\partial Q/\partial \mu$ changes its polarity ($|\mu_{dQ/d\mu=0}|$) for multiple samples. The $|\mu_{Drag=0}|$ and $|\mu_{dQ/d\mu=0}|$ are averaged over the μ values on both electron and hole branches, and represent the half width of the ρ_D peak and the drag layer $\partial Q/\partial \mu$ peak, respectively. The $|\mu_{Drag=0}|$ and $|\mu_{dQ/d\mu=0}|$ values are determined using frictional drag measurements in either bottom or top bilayer graphene from four samples with different interlayer thickness and layer mobility. Furthermore, the data are collected at different drive layer densities, not only at DNP. Figure 4(b) clearly indicates that $|\mu_{Drag=0}|$ agrees very well with $|\mu_{dQ/d\mu=0}|$, suggesting that the overall behavior of the anomalous drag at low T is governed by the drag layer $\partial Q/\partial \mu$. Consistent with Figs. 1 and 2 data we do not find a correlation between the drag resistivity and the drive layer $\partial Q/\partial \mu$.

While reminiscent of energy drag, the giant drag measured here deviates from the simple energy drag picture presented in Ref. [2]. We note that Ref. [2] assumes fully overlapping layers with identical geometries, and contact configurations. In contrast, in the actual devices examined here the geometry and contact configurations of the drive/drag layers are different [Fig. 1(a)]. As a result, anisotropic heat flow due to sample geometry [20] as well as Peltier heating outside of the active layers may contribute to the layer non-reciprocity in our drag measurements. A second ingredient that may lead to non-reciprocity is drive current-induced density gradient in both layers proportional to C_{int}, and to drive layer resistivity. The charge density gradient is not symmetric when interchanging the drive and drag layers, and is largest when the layer with the lower density is used as a drive layer.

The polarity of the energy drag is determined by the sign of potential fluctuations in graphene, $\langle \delta\mu_B \delta\mu_T \rangle$ [2]. A negative drag of thermoelectric origin measured at DNP indicates that $\langle \delta\mu_B \delta\mu_T \rangle < 0$. This suggests that strain [21], rather than charged impurities [22] dominates the density inhomogeneity. For impurity induced inhomogeneity $\langle \delta\mu_B \delta\mu_T \rangle > 0$, and a positive drag is expected at charge neutrality.
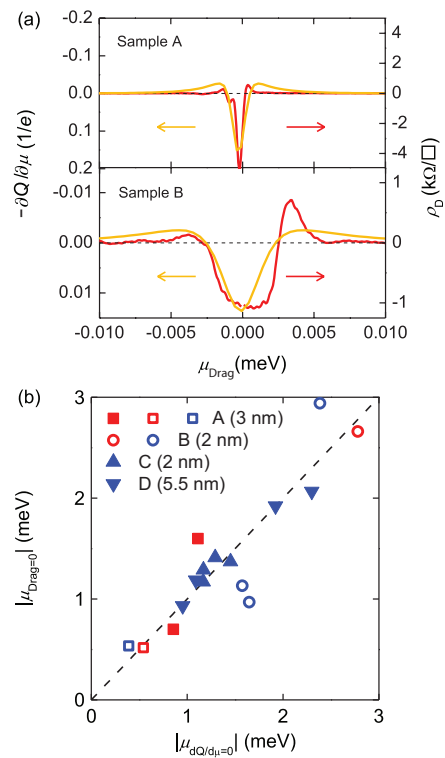

FIG. 4: (a) Drag layer $-\partial Q/\partial \mu$ (yellow) and ρ_D (red) vs. μ_{Drag} in Samples A, and B at $T = 1.5$ K. The data were acquired by sweeping the layer densities such that $n_B = -n_T$. (b) $|\mu_{Drag=0}|$ as a function of $|\mu_{dQ/d\mu=0}|$ of the drag layer for four samples, with different interlayer spacing shown in the legend. The open (closed) symbols mark data measured using the top (bottom) bilayer as drag layer. The red (blue) symbols represent data measured at zero (finite) drive layer density.

Lastly, we discuss similarities and differences between the energy drag previously observed in double monolayer graphene heterostructures [10, 23], and the drag in double bilayer graphene heterostructures. The drag in monolayer graphene shows a peak at the DNP, has a positive value, and is maximum at higher temperatures, $T \simeq 70$ K. The positive drag at DNP is understood as energy drag where impurity induced disorder creates a positive correlation of the layer chemical potential fluctuations $\langle \delta\mu_B \delta\mu_T \rangle$ [2]. Interestingly, a comparison of the monolayer and bilayer graphene Peltier coefficients using Eq. (1) shows that the higher density of states and smaller σ at charge neutrality in bilayer graphene yields a much larger $\partial Q/\partial \mu$, and consequently larger drag at charge neutrality by comparison to monolayer graphene, in agreement with the experimental observations (see Supplementary Material).

In summary, we report an anomalous giant, negative frictional drag $\simeq 1$ kΩ in high mobility double bilayer graphene near the drag layer charge neutrality at temperatures lower than 10 K, with values approaching that of layer resistivity. The drag increases with decreasing

T down to $T = 1.5\,\mathrm{K}$, and does not obey the layer reciprocity. This opens an unanticipated playground for exploring new electron-interaction mediated phenomena in double layer systems even at zero field.

Note added: during the preparation of this manuscript we became aware of a related work described in Ref. [24].

---

[1] J. P. Eisenstein, G. S. Boebinger, L. N. Pfeiffer, K. W. West, and S. He, Phys. Rev. Lett. **68**, 1383 (1992).

[2] J. C. W. Song and L. S. Levitov, Phys. Rev. Lett. **109**, 236602 (2012).

[3] H. Noh, S. Zelakiewicz, T. J. Gramila, L. N. Pfeiffer, and K. W. West, Phys. Rev. B **59**, 13114 (1999).

[4] M. Kellogg, I. B. Spielman, J. P. Eisenstein, L. N. Pfeiffer, and K. W. West, Phys. Rev. Lett. **88**, 126804 (2002).

[5] E. Tutuc, M. Shayegan, and D. A. Huse, Phys. Rev. Lett. **93**, 036802 (2004).

[6] J. P. Eisenstein and A.H. MacDonald, Nature **432**, 691 (2004).

[7] A. F. Croxall, K. Das Gupta, C. A. Nicoll, M. Thangaraj, H. E. Beere, I. Farrer, D.A. Ritchie, and M. Pepper, Phys. Rev. Lett. **101**, 246801 (2008).

[8] J. A. Seamons, C. P. Morath, J. L. Reno, and M. P. Lilly, Phys. Rev. Lett. **102**, 026804 (2009).

[9] S. Kim, I. Jo, J. Nah, Z. Yao, S. K. Banerjee, and E. Tutuc, Phys. Rev. B **83**, 161401(R) (2011).

[10] R. V. Gorbachev, A. K. Geim, M. I. Katsnelson, K. S. Novoselov, T. Tudorovskiy, I.V. Grigorieva, A.H. MacDonald, K. Watanabe, T. Taniguchi, and L. A. Ponomarenko, Nature Phys. **8**, 896 (2012).

[11] A. Gamucci *et al.*, Nature Commun. **5**, 5824 (2014).

[12] A. Perali, D. Neilson, and A. R. Hamilton, Phys. Rev. Lett. **110**, 146803 (2013).

[13] K. Lee, B. Fallahazad, J. Xue, D. C. Dillen, K. Kim, T. Taniguchi, K. Watanabe, and E. Tutuc, Science **345**, 58 (2014).

[14] S. Kim and E. Tutuc, Solid State Commun. **152**, 1283 (2012).

[15] K. Lee, B. Fallahazad, H. Min, and E. Tutuc, IEEE Trans. Electron Devices **60**, 103 (2013).

[16] B. Fallahazad *et al.*, Nano Letters **15**, 428 (2015).

[17] E. McCann and V. I. Fal'ko, Phys. Rev. Lett. **96**, 086805 (2006).

[18] N. W. Ashcroft and N. D. Mermin, Solid State Physics (Brooks Cole, 1976).

[19] Y. M. Zuev, W. Chang, and P. Kim, Phys. Rev. Lett. **102**, 096807 (2009).

[20] J. C. W. Song, L. S. Levitov, Phys. Rev. Lett. **111**, 126601 (2013).

[21] M. Gibertini, A. Tomadin, F. Guinea, M. I. Katsnelson, and M. Polini, Phys. Rev. B , 85 201405 (2012).

[22] J. Xue, J. Sanchez-Yamagishi, D. Bulmash, P. Jacquod, A. Deshpande, K. Watanabe, T. Taniguchi, P. Jarillo-Herrero, and B. J. LeRoy, Nature Mater. **10**, 282 (2011).

[23] M. Titov *et al.*, Phys. Rev. Lett. **111**, 166601 (2013).

[24] J. I. A. Li, T. Taniguchi, K. Watanabe, J. Hone, A. Levchenko, C. R. Dean, arXiv:1602.01039 (2016).